applied sciences

MDPI

Article

Optical Module for Simultaneous Crop Cultivation and Solar Energy Generation: Design, Analysis, and Experimental Validation

Jinwoo Jung [1], Young-Jae Kim [2], Hyun-Sang Shin [3], Ki-Joong Kim [3], Bu-Hyun Shin [3], Sang-Wook Lee [4], Byung-Wook Kim [5,*] and Wan-Chin Kim [6,*]

[1] Department of Robotics Engineering, Daegu Catholic University, 13-13, Hayang-ro, Hayang-eup, Gyeongsan-si 38430, Republic of Korea
[2] YNDK, Research2-267, 169-148, Gwahak-ro, Yuseong-gu, Daejeon 34027, Republic of Korea
[3] Department of Mechanical Engineering, Hanbat National University, 125, Dongseo-daero, Yuseong-gu, Daejeon 34158, Republic of Korea
[4] School of Mechanical Engineering, Wonkwang University, 460, Iksan-daero, Iksan 54538, Republic of Korea
[5] Iproptics, 100, Artcenter-daero 168 beon-gil, Yeonsu-gu, Incheon 22006, Republic of Korea
[6] Department of Mechanics-Material Convergence System Engineering, Hanbat National University, 125, Dongseo-daero, Yuseong-gu, Daejeon 34158, Republic of Korea
* Correspondence: proptics77@iproptics.com (B.-W.K.); wckim97@hanbat.ac.kr (W.-C.K.)

Abstract: This study proposes a rectangular-shaped optical module capable of simultaneously implementing crop cultivation and solar power generation. By employing a cylindrical Fresnel lens (CFL) array plate with a size of 100 × 100 mm^2, multiple focal lines are formed, where some of the incident light transmits through the module while the rest is guided laterally through the rectangular lightguide structure. This guided sunlight is then concentrated by a cylindrical compound parabolic concentrator (CCPC) structure, resulting in a 20-fold concentration ratio, onto a 5 × 100 mm^2 Si photovoltaic (PV) cell. To experimentally verify feasibility, both the CFL array plate and the lightguide plate were fabricated with three-axis machine tooling equipment and assembled. The power generated experimentally by the 5 × 100 mm^2 Si PV cell was 54% of the expected value from the simulation results on the light-concentrated efficiency considering experimental conditions, while the results on experimental transmittance along with rotation angles were very close to the simulation results. However, overall, the tendency of the generated power along the rotation angles is close to the tendency of the light-concentrated efficiency along the rotation angles from the simulation. Additionally, this study dealt with further consideration to enhance light-concentrated efficiency, introducing a means to adjust the trade-off relationship between transmittance and light-concentrated efficiency.

Keywords: agrivoltaic solution; transmissive light-concentrating optical module; cylindrical Fresnel lens (CFL); cylindrical compound parabolic concentrator (CCPC); Si photovoltaic cell (Si PV cell)

check for updates

Citation: Jung, J.; Kim, Y.-J.; Shin, H.-S.; Kim, K.-J.; Shin, B.-H.; Lee, S.-W.; Kim, B.-W.; Kim, W.-C. Optical Module for Simultaneous Crop Cultivation and Solar Energy Generation: Design, Analysis, and Experimental Validation. *Appl. Sci.* **2024**, *14*, 4758. https://doi.org/10.3390/app14114758

Academic Editor: Nunzio Cennamo

Received: 15 April 2024
Revised: 22 May 2024
Accepted: 29 May 2024
Published: 31 May 2024

Copyright: © 2024 by the authors. Licensee MDPI, Basel, Switzerland. This article is an open access article distributed under the terms and conditions of the Creative Commons Attribution (CC BY) license (https://creativecommons.org/licenses/by/4.0/).

1. Introduction

The essential resources of humanity, such as water, energy, and food, are facing a rapid increase in global demand due to the expected rapid population growth to 9.7 billion by 2050. However, difficulties are anticipated in sustaining resource production to meet such demand [1–5]. According to the Food and Agriculture Organization (FAO), agricultural production in developing countries needs to double to meet demand, and these nations are predicted to face competition for water and energy resources as well as the impacts of climate change [6]. Irrigation involves controlling the water demand that is not met by rainfall through artificial systems to facilitate crop growth and development [7]. Securing energy for irrigation is crucial for agricultural development in developing countries with insufficient rainfall. Therefore, it is necessary to actively utilize environmentally friendly and cost-effective renewable energy sources, with solar photovoltaic (PV) panels being

used for solar power generation [8,9]. Globally, renewable energy accounts for 20% of total energy consumption, with approximately 30% of renewable energy investments allocated to wind energy and 60% to solar energy [10]. It is projected that 25% of the world's required power will be obtained through solar power generation by 2050 [10]. However, utilizing solar power generation for irrigation presents challenges due to the significant land area occupied by solar panels, potentially reducing arable land [11].

To mitigate these issues, efforts are being made to introduce agrivoltaic systems. Agrivoltaic systems aim to establish systems where solar panels and cultivation can coexist, with the core concept being the utilization of the space beneath solar panels for agricultural purposes [12–14]. Studies, such as that by Jamil et al., have reported that applying agrivoltaic methods to just 1% of Canada's farmland could satisfy at least a quarter of the nation's electricity demand [15]. However, research on agrivoltaic systems primarily focuses on determining optimal panel arrangements based on factors such as the amount of light reaching crops beneath PV arrays and the shaded land area of PV cells [16]. This approach often incurs significant costs in constructing and maintaining overall solar panel arrays and does not fully resolve the trade-offs between agriculture and solar power generation.

Another approach being explored is the use of semitransparent organic solar cells (STOSCs) for combined solar power generation and cultivation [17–19]. Agrivoltaic systems typically use Si PV cells, which offer high energy conversion efficiency and stability but are costly and render shaded land areas unusable for cultivation. In contrast, STOSCs offer a way to utilize solar spectra other than those needed for plant photosynthesis within the same land area. STOSCs contain an active layer that generates electron-hole pairs, covered with a transparent conductive material allowing certain spectra to penetrate. Thus, photons in the visible spectrum necessary for photosynthesis pass through, while photons in the UV and near-infrared spectrum are converted into electrons. Compared to Si solar cells, STOSCs with thin-film structures are lighter and cheaper to manufacture. However, their semi-transparency poses a trade-off between power conversion efficiency (PCE) and average visible transmittance (AVT), and they may lack durability in various environmental conditions compared to Si PV systems [20,21].

The agrivoltaic system faces several challenges. It is not feasible to combine solar power generation and crop cultivation on the same land, and setting up a large-scale solar power generation system is expensive due to the need for costly high-efficiency single-crystal Si PV cells and dual-axis tracking to account for daily and seasonal variations in solar light angle. These challenges limit the available land for cultivation and hinder cost reduction in manufacturing and operating solar power generation systems. Although research on combining solar power generation and cultivation using STOSCs is ongoing, the PCE and AVT of the state of the art are 11% and 28% [22], which is insufficient for crops requiring significant solar radiation. Additionally, STOSCs require continuous improvement in device and module durability. To address these issues, our study aimed to develop an optical module capable of higher AVT while using small-sized Si PV cells for electricity generation. To achieve our aim, we propose an optical system composed of a thin cylindrical Fresnel lens (CFL) array plate and a compact lightguide plate. Basically, in the proposed system, PCE and AVT vary depending on the incident angle of sunlight. We believe that our approach can be one of the solutions to reduce the size of expensive Si solar cells and enable the growth of crops requiring high solar radiation. In this paper, we report the results of its design and fabrication, as well as experimental results on the module's transmittance and generated power efficiency, comparing them with detailed simulation results.

2. Design and Analysis of the Proposed Optical System

2.1. Design of the Proposed Optical System

Figure 1 illustrates a schematic diagram of the proposed optical system. Initially, solar lightflux is concentrated into multiple linear light beams using a CFL array. The linearly concentrated lightflux is then reflected by multiple prism-shaped geometries formed on

the exit surface of the lightguide, and reflected lightflux is guided towards the edge of the lightguide by internal reflection in the lightguide. Table 1 presents the design specifications of the CFL array plate. Increasing the pitch of the CFL array results in a greater overall thickness of the optical module to enhance the efficiency at the focal plane of the CFL. To compact the optical module comprising the CFL array plate and the lightguide while maintaining high optical efficiency at the focal plane of the CFL, the pitch and the focal length of the CFL array were set to 10 mm and 11.5 mm, respectively. The CFL array plate consists of 10 CFLs arranged in an array, with a width of 100 mm and a length ensuring a square entrance cross-section of 100 mm. The design wavelength of the CFL was set to 550 nm, the central wavelength of the visible spectrum, which corresponds to the maximum range of solar spectral irradiance. Polymethyl methacrylate (PMMA) with a refractive index of 1.4936 at the design wavelength was considered as the material for the CFL.

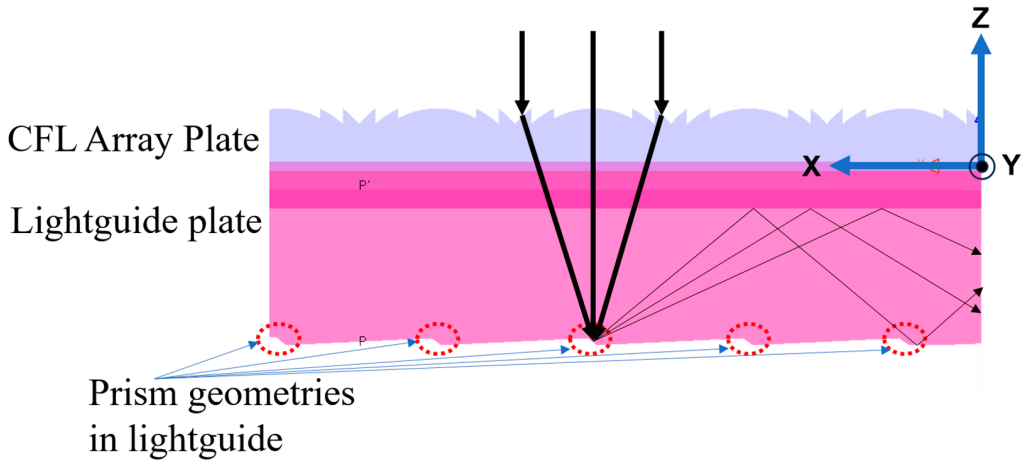


Figure 1. Concept of the proposed optical layout.

To analyze the concentration efficiency of the CFL array plate with specifications similar to Table 1, non-sequential ray tracing simulations were conducted using LightTools™ (Synopsys, Sunnyvale, CA, USA). During the analysis, solar spectrum data corresponding to the Phoenix (USA) region (latitude 33.5°, longitude −112.17°) provided by LightTools™ was applied as the spectrum data for the light source [23]. Additionally, the size of the sunlight-simulating light source was set to 10,000 mm^2 to match the size of the CFL array plate. Considering the size of the CFL array plate and the angle of incidence of solar radiation, the distance from the CFL array plate to the light source was set to 16,205 mm. Furthermore, the radiant flux of the sunlight-simulating light source was set to 5 W, proportional to the irradiated area of 10,000 mm^2, and directed to the designed CFL array plate entrance surface. Figure 2 illustrates the results of non-sequential ray tracing analysis of the radiant flux transmitted to the focal plane of the CFL array plate under direct normal incidence (DNI) conditions. This analysis considered transmission and reflection due to the Fresnel loss of the CFL array plate. As shown in Figure 2, a cylindrical focused line array is formed 11.5 mm below the CFL array plate, and it can be observed that some of the incident light flux is reflected and lost at each entrance and exit interface of the CFL array plate. The total radiant flux reaching the focal plane of the designed CFL array plate is 4.6 W, resulting in an optical transmission efficiency of 92% when considering the 5 W of incident radiant flux. The radiant flux reaching the focal area of the CFL array, represented by the blue-line box, is 4.2 W, indicating an optical transmission efficiency of 84% for the CFL array plate.

Table 1. Design specification of the cylindrical Fresnel lens (CFL) array plate.

Parameter	Unit	Target	Remark
Pitch	mm	10	CFL array plate with the dimension of 100×100 mm^2. The plate is composed of 10 CFL structures
Width	mm	100	
Length	mm	100	
Designed wavelength	nm	550	Considering the peak of the solar spectrum
Refractive index	–	1.4936	Refractive index at 550 nm of PMMA
Effective focal length	mm	11.5	Considering a compact optical module
Optical power efficiency	%	>80	Considering the Fresnel loss of CFL array plate

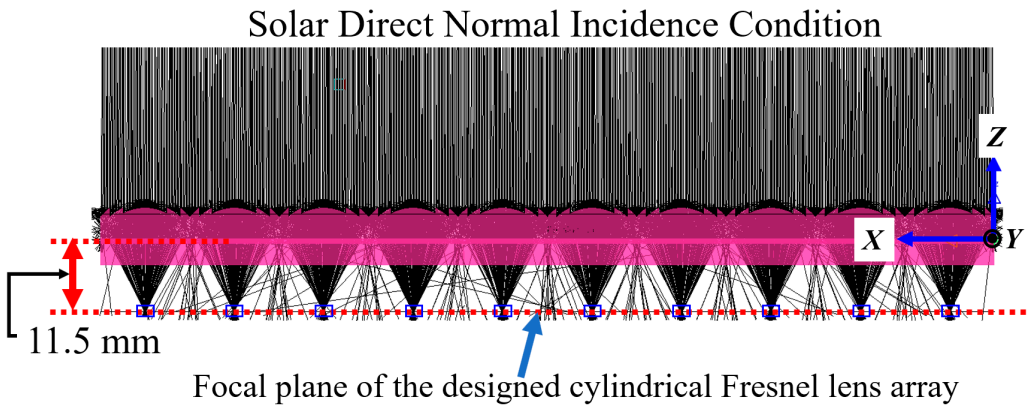


Figure 2. Non-sequential ray tracing for the designed CFL array plate with the solar direct normal incidence (DNI) condition.

To transmit the light flux reaching the focal area of the CFL array to the edge of the lightguide, it is necessary to form a lightguide with a prism-shaped exit surface near the focal area of the CFL array, as depicted in Figure 1. In this study, we considered a lightguide with the same cross-sectional area as the CFL array plate, and a thickness of 10 mm. The angle of the prism shape was set to 40° to maximize the transmission of light flux to the lightguide edge.

In this study, we also explored ways to reduce the usage area of high-cost Si PV cells. To satisfy a concentration ratio of 20, where solar flux entering an area of 100 mm × 100 mm is concentrated onto a Si PV cell measuring 5 mm × 100 mm, the light flux guided to the edge of the lightguide is directed to the cylindrical compound parabolic concentrator (CCPC) end face by a CCPC structure. Figure 3 illustrates the cross-sectional shape of the CCPC and the parameters defining its shape. The relationship between the maximum acceptance angle and the parameters of the CPC shape is defined by Equation (1), and in this study, considering a maximum acceptance angle, $\theta_i = 27°$, and both $b_1 = 10$ mm and $b_2 = 5$ mm, the x-axis length of the CCPC, L, was set to 14.7 mm [24].

$$\tan\theta_i = \frac{b_1 + b_2}{2L} \quad (1)$$

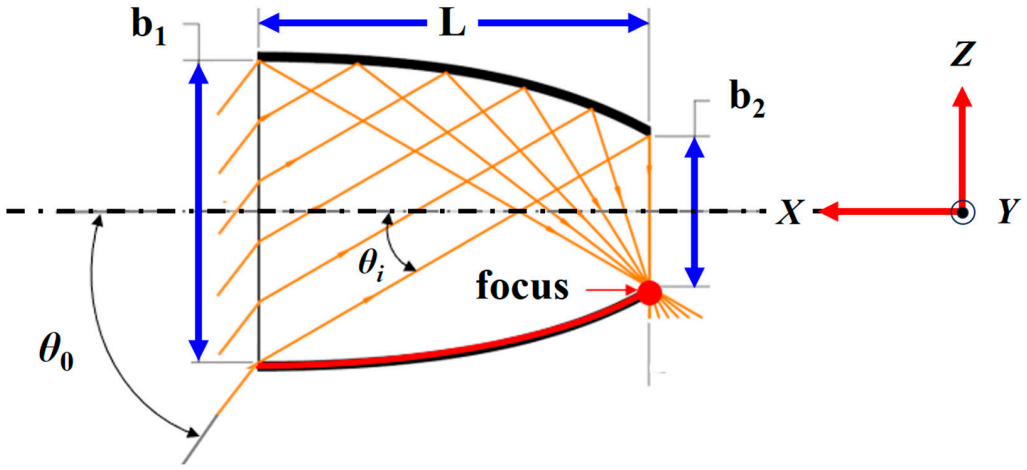


Figure 3. Cross-sectional shape and parameters of the compound parabolic concentrator (CPC).

2.2. Primary Analysis of the Designed Optical Module

Figure 4 illustrates the overall shape and dimensions of the designed optical module, including its key components. As it is convenient to fabricate the CFL array plate and the lightguide separately, it is necessary to set an appropriate air-gap spacing distance, ΔS, for assembly. For this purpose, we examined the light power incident on the CCPC end surface according to the magnitude of ΔS. In this analysis, the transmittance and reflection due to the Fresnel loss were considered for both the CFL array plate and the lightguide. Figure 5 represents the transmitted power through the module and the concentrated power on the CCPC end surface according to the ΔS values. When ΔS was set to 1.3 mm, the concentrated light power on the CCPC end surface reached its maximum value of 1.475 W. At this point, considering the 5 W radiative power of the solar simulating light source, the transmittance through the optical module and the concentrated optical efficiency on the CCPC end surface were 54.1% and 29.5%, respectively.

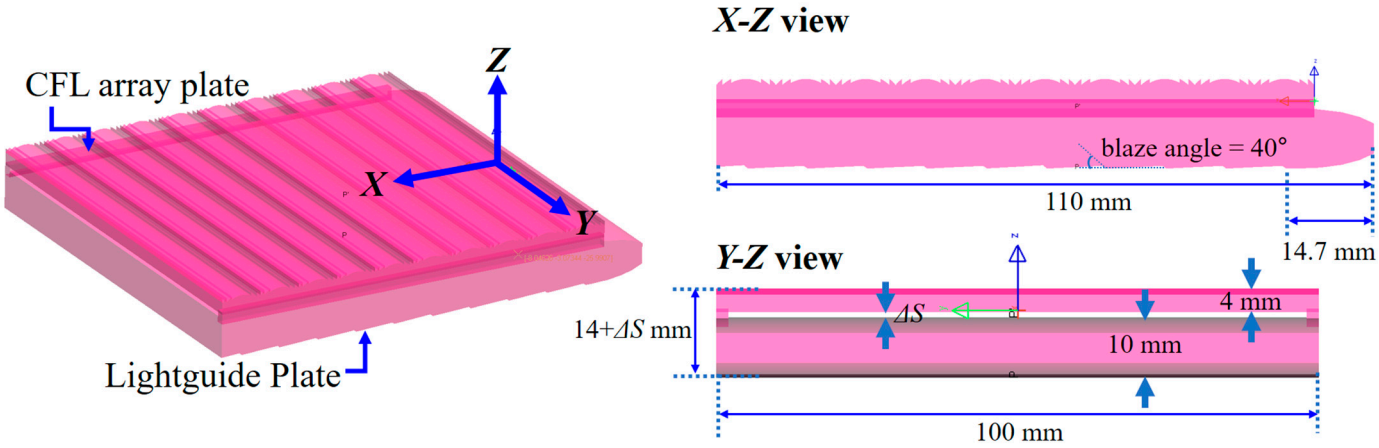


Figure 4. Shape and dimensions of the designed transmissive light-concentrating optical module.

The designed optical module considers tracking the annual variation of the incidence angle of the sun, while not tracking the daily variation. In Figure 6, the angle notations for the rotation directions of the sun are defined. α and β represent the incidence angle of the sun in the direction of daily variation and the incidence angle in the direction of annual variation, respectively, for the normal incident surface of the optical module. Thus, when both α and β are 0°, it is under DNI conditions. Considering tracking the annual variation of the incidence angle of the sun, when tracking without error, β is always 0°. However, to examine the allowable tracking error, the transmittance and the concentrated

light efficiency of the module were analyzed for β variations. Figure 7 illustrates the power transmitted through the module and the concentrated power on the CCPC end surface according to changes in α and β when the incident solar power onto the CFL array plate is set to 5 W. In this simulation, we set the range of α considering the range of α where the amount of light transmitted to the CCPC end is more than 30% of its maximum value. As shown in Figure 7a, within the range of $|\alpha| < 15^\circ$ for the daily variation in the incidence angle of the sun, 28% of the incident solar power can be concentrated onto the CCPC end surface, and it can concentrate more than 16% up to $|\alpha| < 20^\circ$. At this point, the power transmitted through the module showed more than 50% transmittance within the range of $|\alpha| < 40^\circ$. As shown in Figure 7b, for the annual variation of the incidence angle, more than 28% of the incident solar power can be concentrated onto the CCPC end surface within the range of $|\beta| < 1^\circ$, and it can concentrate more than 15% within the range of $1^\circ < |\beta| < 2^\circ$. The reason for the sharp decrease in concentration efficiency onto the CCPC end surface for the annual variation in the incidence angle of the sun is due to the sun crossing the array direction of the CFL array, causing the incident angle onto the array axis to change.

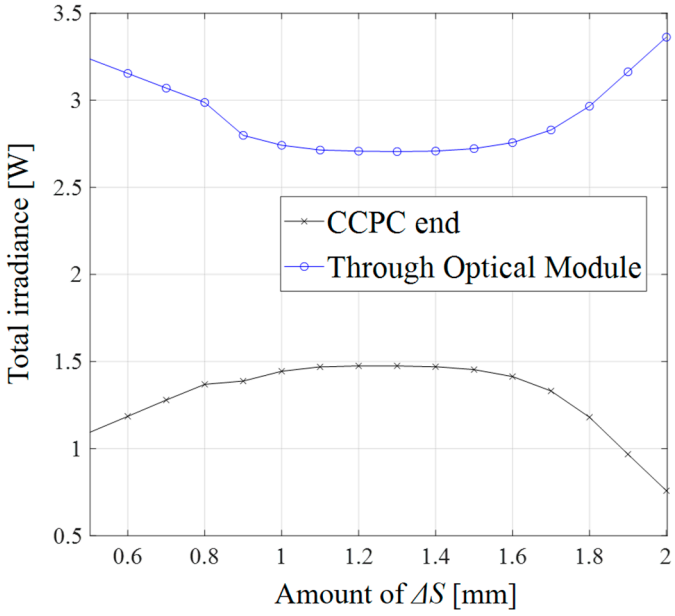


Figure 5. Transmitted power through the module and the concentrated power on the CCPC end surface according to the amount of ΔS.

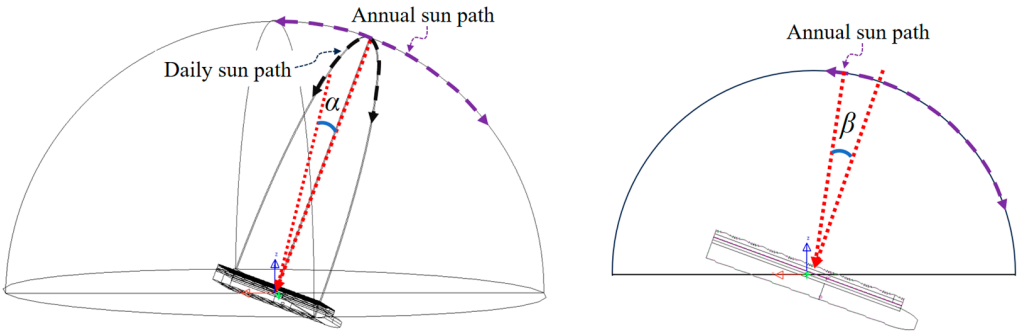


Figure 6. Definition of solar light incidence angle considering daily and annual sun path.

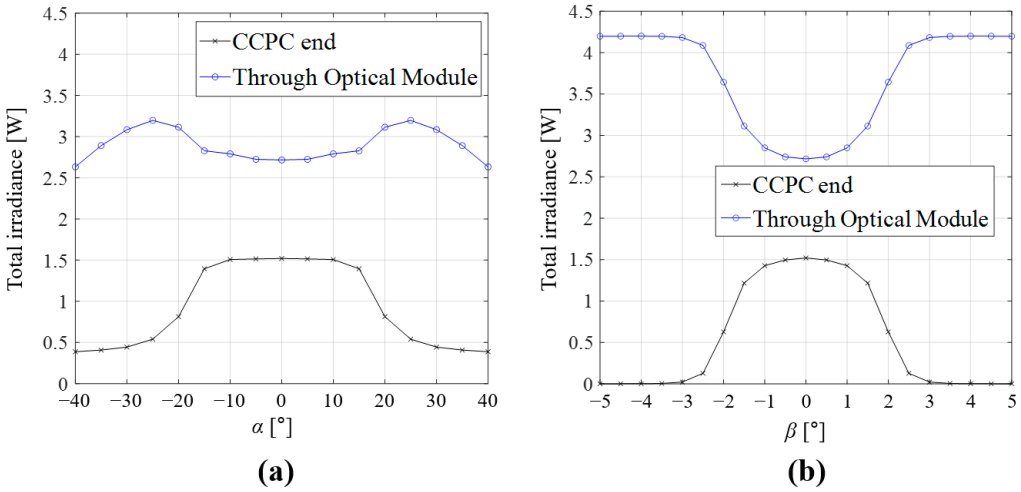


Figure 7. Transmitted power through the module and the concentrated power on the CCPC end along with α and β: (**a**) result of variation in α and (**b**) result of variation in β.

3. Development of the Designed Optical Module

To validate the operating principle of the optical module designed in this study, a 3-axis machine tooling equipment, VM 6500 (DN solutions, Changwon-si, Republic of Korea), was used to manufacture the CFL array plate and lightguide plate. However, when designing the CFL array plate, although the ideal shape of a cylindrical Fresnel lens was considered, the machining freedom of the device was not high enough to properly implement the vertical walls of each zone of the Fresnel lens. Therefore, as shown in Figure 8a, the draft angle of each zone was changed to 20° for manufacturing. Figure 8b illustrates the shape of the CFL array plate and the modified design shape together. As shown in Figure 8b, while the pitch of the manufactured CFL array, the radius to each zone, and the wall angle of each zone were generally well implemented, fillet curvature occurred at the corners of each zone.

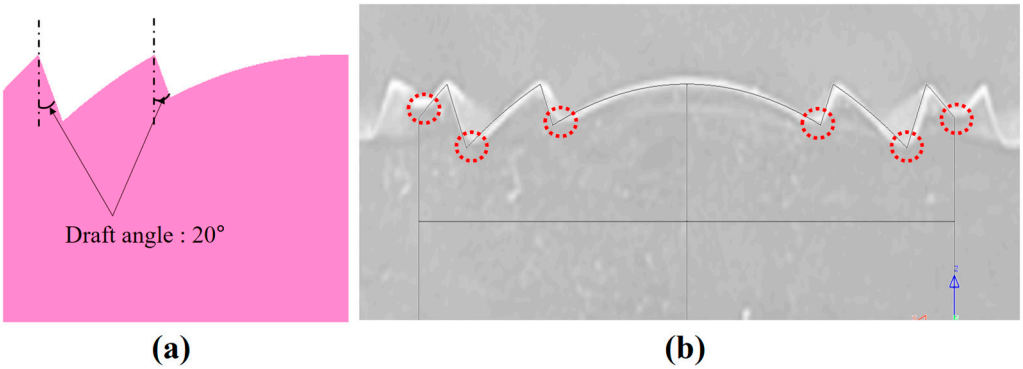


Figure 8. Modified design of CFL (**a**) and its fabrication result with the designed profile (**b**).

A photograph of the assembled optical module prototype, consisting of the machined CFL array plate and the lightguide plate integrated with the CCPC, is presented in Figure 9. As ΔS was set to 1.3 mm in the designed optical module shown in Figure 4, the total thickness of the module is 15.3 mm, while the thickness of the manufactured optical module ranged from approximately 15.25 to 15.27 mm. Taking the fabrication errors of the CFL shape and the thickness deviation of the optical module into account, the key parameters were recalculated according to the variations in α and β. In this analysis, for the shape of CFL, draft angles and edge fillet radii were set to 20° and 0.1 mm, respectively. Figure 10 illustrates the transmittance through the module and light concentration efficiency

as a percentage of the incident optical power of 5 W, compared to the characteristics of an ideal optical module.

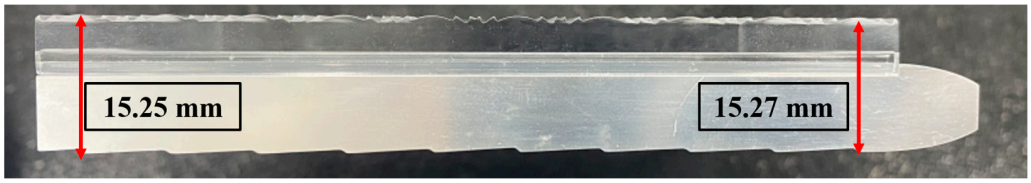


Figure 9. Assembled optical module prototype.

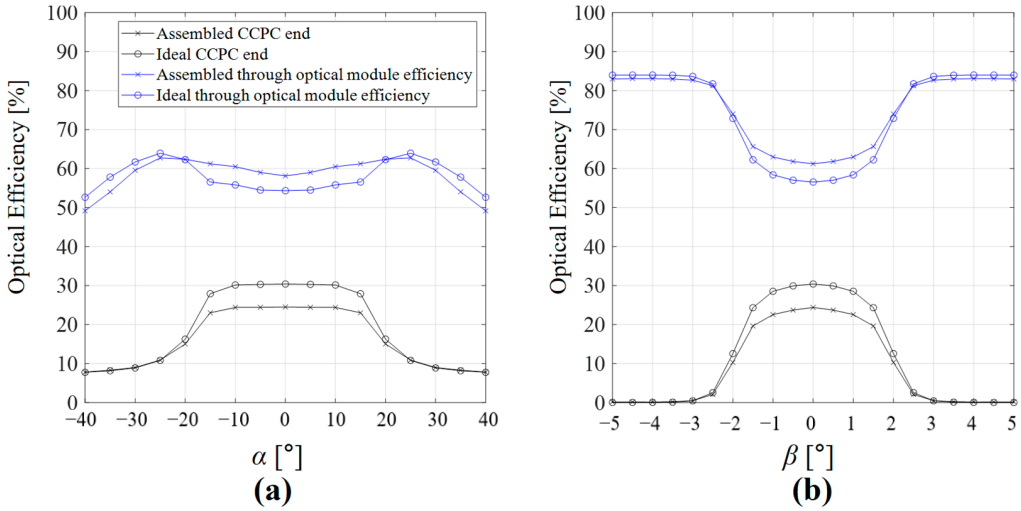


Figure 10. Transmittance through the module and the concentrated optical power efficiency on the CCPC end surface according to variation in the incidence angle of the sun, considering fabrication error of the CFL module: (**a**) result of variation in α and (**b**) result of variation in β.

Comparing to the results of the ideal module, the optical module considering fabrication deviations reveals that there is approximately a 5% decrease in the concentrated optical efficiency at the CCPC end surface for α and β variations in the maximum efficiency range, $|\alpha| < 15°$ and $|\beta| < 1.5°$. Furthermore, compared to the results for the ideal module, the transmittance through the module shows a similar level of transmittance for α variations within the range of $|\alpha| < 40°$, while for β variations, it exhibits approximately a 5% higher transmittance in the minimum transmittance range of $|\beta| < 1.5°$.

4. Experimental Results and Discussion

The solar radiation spectrum data used in the design of the optical module does not match the local solar radiation conditions in the laboratory, and accurate radiation spectra considering the local weather conditions are not known. Therefore, to experimentally measure the through-module transmittance and power generation, a high-power white LED illumination device was used. In this study, a high-power white light LED with a color temperature of 6500 K and a radiant output of 2420 lm, CXB1520 from Cree LED (Durham, NC, USA), along with two lenses, was used for illumination. Figure 11 illustrates the applied LED radiation spectrum and the experimental concept for measuring the transmittance and power generation of the fabricated module. The emitted light from the illumination device equipped with converging lenses is incident on the fabricated optical module placed 3 m ahead. In the experiment, we used the monocrystalline p-type silicon photovoltaic (Si PV) cell, SCM 5WE-6V from Solarcenter (Gimpo-si, Republic of Korea). It was attached to the CCPC end surface, which has an area of 5 mm × 100 mm, using a transparent encapsulant, Sylgard-184 from DOW (Midland, MI, USA). Before the experiment, considering the fabrication deviations of the optical module and experimental

conditions, the through-module transmittance and the concentrated power efficiency on the CCPC end surface and the incident surface of the Si PV cell were predicted. In the results shown in Figure 12, the illumination device consisting of an LED light source and two lenses as presented in Figure 11 were considered, and the thickness of the transparent encapsulant was set to 0.1 mm. Since a commercially available illumination device was used, the specifications of the two lenses were not precisely known, so we modeled them based on data measured by a surface profiler.

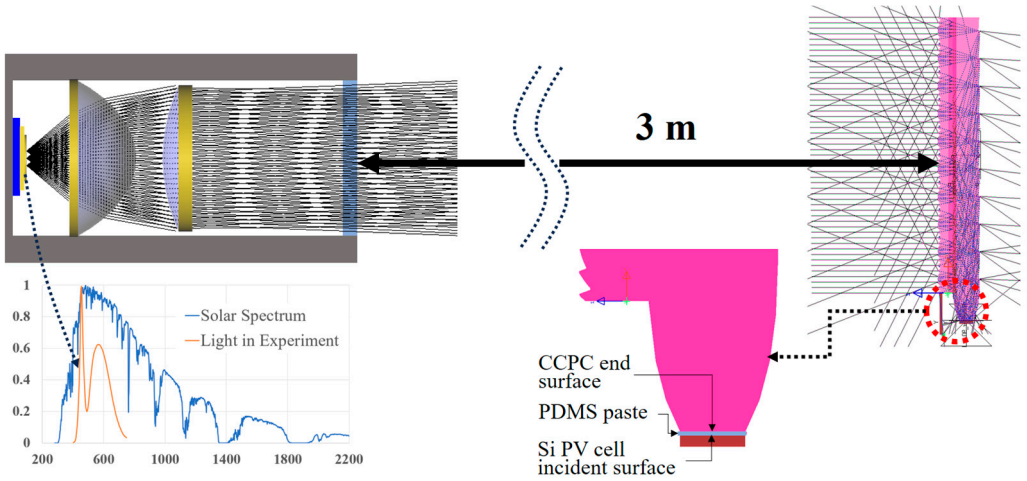


Figure 11. Experimental concept for measuring the through-module transmittance and the generated electrical power using the concentrated solar power in Si PV cell.

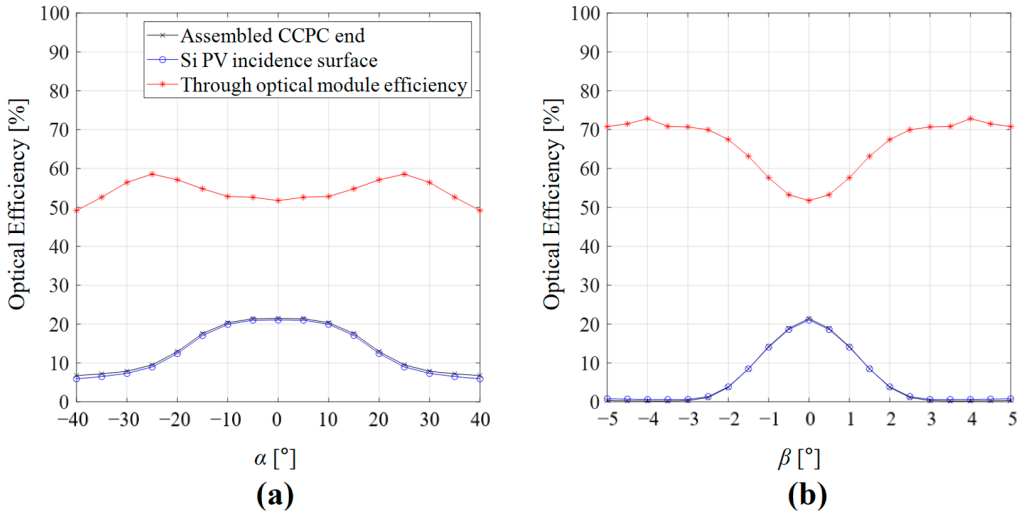


Figure 12. Transmittance through the module and the concentrated optical power efficiency on the CCPC end surface and the incident surface of the Si PV cell according to variation in the incidence angle of the sun, considering experimental conditions: (**a**) result of variation in α and (**b**) result of variation in β.

Comparing with the results shown in Figure 10, it can be observed that, on average, the transmittance and the concentrated power efficiency decreased by approximately 3.8% and 2.4%, respectively, for the rotation angle α. However, the overall trends of transmittance and the concentrated power efficiency were very similar. For the rotation angle β, both parameters are more sensitively changed compared to the results shown in Figure 10. This is because, for the approximate solar source of 16,205 mm, the incident angle of all light incident on the module is close to 0°. However, under experimental conditions, considering a distance of 3 m between the illumination device and the module, the incident angle

ranges from 0° to 1.9°, and the sensitivity of the rotation direction β is higher than that of the rotation direction α.

To experimentally measure the module transmittance and compare the simulation results, we first measured the reference illuminance at a distance of 3 m in front of the illumination device in the absence of the fabricated optical module. The measured reference illuminance at 3 m in front of the illumination device was 106 lx. Using the prototype optical module, the module transmitting illuminance was measured by rotating it in the α and β directions around the center position of the CFL array plate. Then, the transmittance was calculated as a percentage of the reference illuminance. To measure the concentrated power efficiency, we used a PV cell with an effective area larger than 100 mm × 100 mm. In the absence of the optical module, the reference generated power was measured in the 100 mm × 100 mm PV area arranged perpendicular to the optical axis at 3 m in front and was set as the reference power for calculating the concentrated power efficiency. As shown in Figure 13a, as the size of the PV cell is larger than 100 mm × 100 mm, a 100 mm × 100 mm aperture plate was attached to the incident surface of the PV cell. The measured reference generated power was 22 μW. To measure the generated power with the proto-optical module, a PV cell with a 100 mm × 5 mm aperture plate was attached to the incident surface of the PV cell, as shown in Figure 13b. An optical module was attached to the PV cell using a transparent encapsulant. Under these conditions, the generated power while rotating the proto-optical module in the α and β directions around the center position of the CFL array plate was measured. In Figure 14, the measured module-transmitted illuminance and the measured generated power according to the rotation angles are shown as a percentage of each standard value.

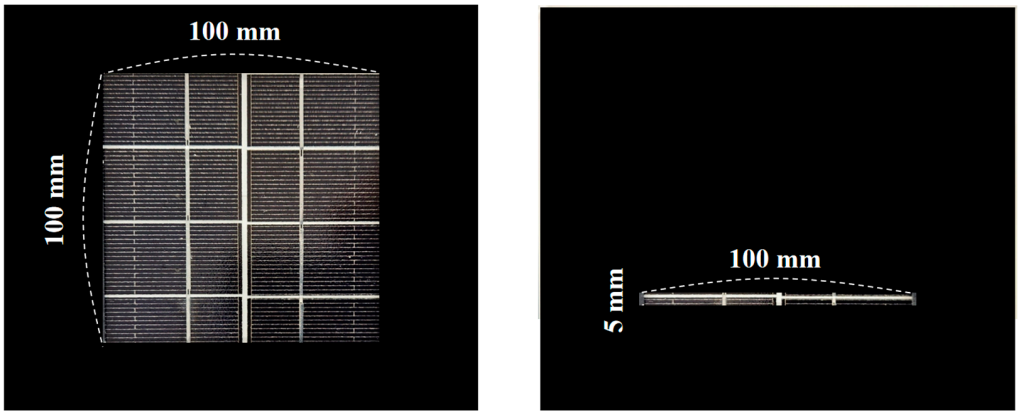


Figure 13. Apertured PV cell to measure generated electricity: (**a**) the apertured PV cell with a clear aperture of 100 mm × 100 mm and (**b**) the apertured PV cell with a clear aperture of 5 mm × 100 mm.

Comparing the results of the optical module transmittance according to the rotation angle shown in Figure 14a with the simulation results presented in Figure 12, it can be observed that a very similar trend is evident within the angular range of $|\alpha| < 35°$ and $|\beta| < 3°$. When both rotation angles α and β were 0°, the measured illuminance was 57 lx, corresponding to 53.8% of the measured reference illuminance,106 lx. Near $|\alpha| = 25°$, the maximum transmittance of 55% was measured. As $|\beta|$ increases, the transmittance continues to increase steadily, reaching up to 70%, which is similar to the maximum transmittance value shown in Figure 12b. For the generated power from the 5 mm × 100 mm Si PV cell, the maximum value of 2.52 μW was measured when both rotation angles α and β were 0°, representing 11.5% of the reference generated power, 22 μW. Considering the maximum concentrated optical power efficiency, 21.4%, presented in Figure 12, this value is about 54% of the expected value. However, it was confirmed that the overall rotation angle-dependent tendency of the measured module transmittance and

the concentrated optical power efficiency are very similar to the results shown in Figure 12. There can be several reasons for the result that the generated power is lower than expected values from simulations. One major factor could be the inaccurate modeling of the applied illumination device and fabrication errors of the proto-optical module. Another significant factor is that, as illustrated in Figure 13b, the area of the aluminum electrode within the effective area of the PV cell attached to the CCPC end surface using encapsulant is relatively larger compared to the PV cell with the effective aperture of 100 mm × 100 mm shown in Figure 13a. We judged that it induced about a 25% decrease in the generated power.

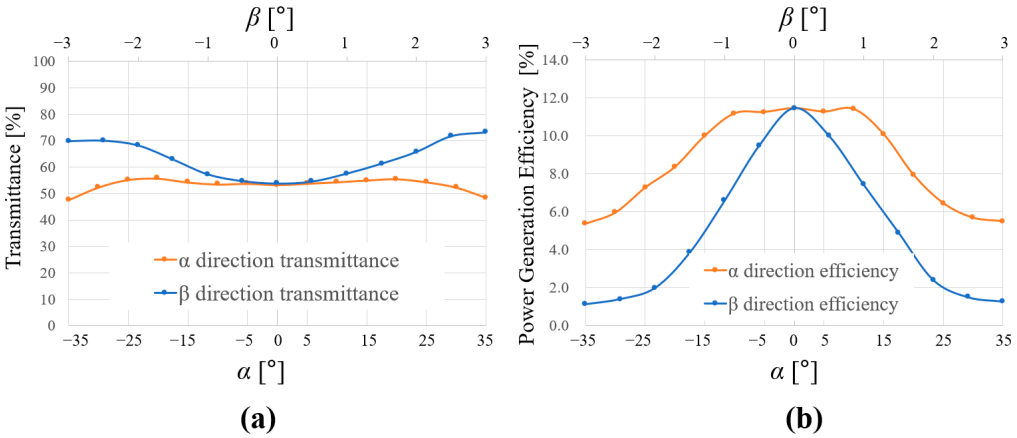


Figure 14. Transmittance through the module and the measured power efficiency on the CCPC end surface and the incident surface of the Si PV cell according to variation in the incidence angle of the sun, considering experimental conditions: (**a**) transmittance through the module and (**b**) generated power efficiency.

In this study, additional investigations were conducted on the structure that could improve the concentration efficiency of the CCPC end surface. In the structure examined through design and experiment, the prism-shaped array at the exit surface of the lightguide was not treated as the reflective surface. The description in Figure 2 indicated that the focused light efficiency formed on the focal plane by the CFL array plate was 84% of the incident optical power. However, as shown in Figure 7a, the module transmittance was about 55% under the DNI condition of $\alpha = 0^\circ$ and $\beta = 0^\circ$. This means that approximately 65% of the incident light power was transmitted through the optical module. Therefore, we conceived that it is feasible to improve the light concentration efficiency to the CCPC end surface by applying a reflective coating to the prism geometry interface, as shown in Figure 15.

In the illumination analysis model, all optical surfaces except those represented as "reflective coated surfaces" in Figure 15 were set as transmission and reflection surfaces considering Fresnel loss. Figure 16 shows the module transmittance and concentrated optical power efficiency to the CCPC end surface of the modified model. In this simulation, the draft angle and the fillet radius of the CFL were set to 20° and 0.1 mm, respectively. The result shows the light concentration efficiency to the CCPC end surface higher than 2 times that of the "assembled CCPC end" shown in Figure 10 in the angular regions of $|\alpha| < 20^\circ$ and $|\beta| < 1.5^\circ$. The transmittance in the regions of $|\alpha| < 20^\circ$ and $|\beta| < 1.5^\circ$ decreased to approximately 35% compared to the results in Figure 10. The magnitudes of the CCPC end surface concentration efficiency and module transmittance are trade-off characteristics, and adjusting the number of surfaces applying the reflective coating in the linear prism geometry of the lightguide can adjust both result characteristics.

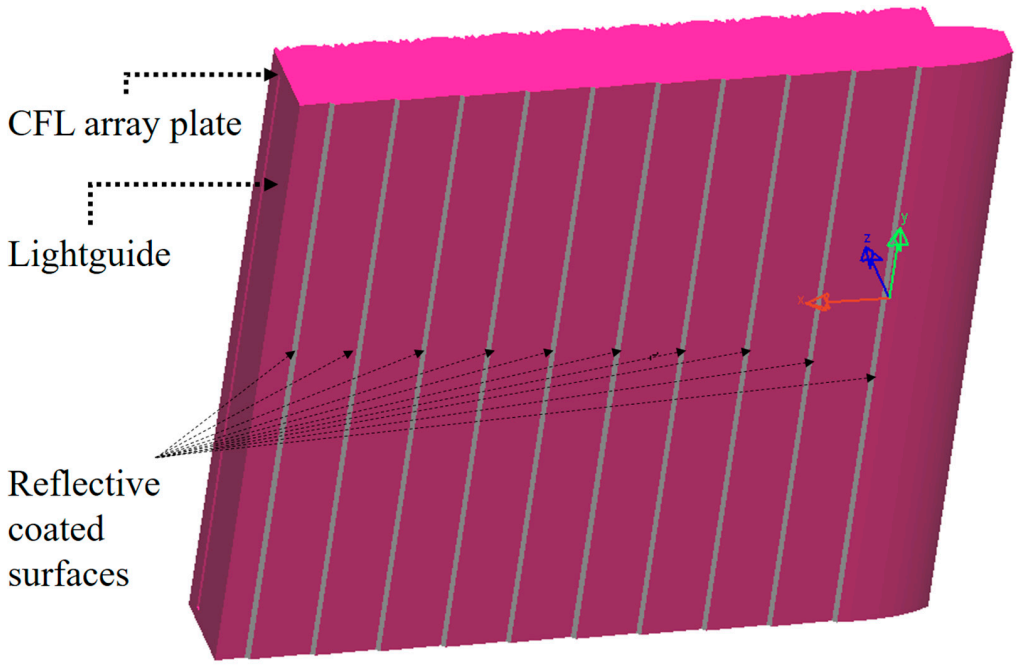


Figure 15. Modified shape of the optical module with reflective coated surfaces on the prism-shaped surfaces of the lightguide.

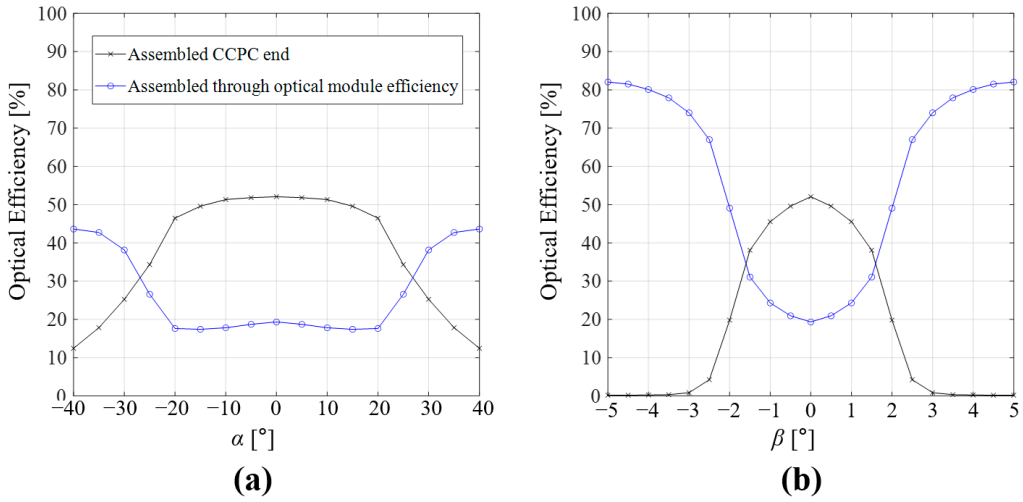


Figure 16. M Transmittance through the module and the concentrated optical power efficiency on the CCPC end surface according to variation in the incidence angle of the sun, of the modified optical module: (**a**) result of variation in α and (**b**) result of variation in β.

In this study, to validate the transmittance and the light collection characteristics of the proposed optical module structure, we designed and fabricated a small-sized unit module with a dimension of 100 mm (X) × 100 mm (Y), a suitable size for the fabrication of the prototype. However, for practical implementation of large-scale simultaneous cultivation-power generation systems based on the devised structure, reducing manufacturing costs by producing larger unit modules and arranging them in an array format is deemed feasible. For instance, by manufacturing unit modules of size 100 (X) mm × 200 (Y) mm using injection molding, it is possible to produce them for less than 4 USD, considering assembly costs even for mass production. In this case, the size of Si PV cells arranged on the CPC-shaped aspect is 5 mm × 200 mm. Meanwhile, the unit cost of high-efficiency mono-crystalline Si PV cells is around 1.0 ~ 1.5 USD/W, with a power output of 4 W for PV-cell modules measuring 100 (X) mm × 200 (Y) mm. Considering this, the material

cost of high-efficiency mono-crystalline Si PV cells with the same area is approximately 4 ~ 6 USD. Ultimately, this is comparable to the material cost of the optical module capable of simultaneous cultivation-power generation proposed in this study. If the proposed optical module is used, compatibility issues related to power transmission are not expected since the same mono-crystalline Si PV cells can be applied. Additionally, conventional PV systems utilizing Si PV cells require dual-axis tracking for seasonal and daily variations in solar incidence angles. While variations exist depending on the country and region, they generate power for approximately 3.5 ~ 4 h per day on average. Suppose the solar incidence angle during the central time of the power generation period meets the DNI conditions by setting the reference angle of the optical module. In that case, the variation range of solar incidence angles during the power generation period is within $|\alpha| < 15^\circ$ [25,26]. Therefore, based on the analysis and experimental results, it is suggested that the module proposed in this study, with a concentration efficiency variation within $|\alpha| < 15^\circ$ of daily solar incidence angle variation, within 15%, may not require tracking means for this purpose. It is also anticipated that tracking methods for seasonal variation in solar incidence angles will be applied similarly to conventional methods.

5. Summary and Conclusions

Our study aimed to develop an optical module capable of higher AVT while using small-sized Si PV cells for electricity generation. We proposed an optical system comprising a thin cylindrical Fresnel lens (CFL) array plate and a compact lightguide plate.

Considering the ideal optical module design proposed in this study, the module transmittance and light concentration efficiency at the CCPC end surface were 55% and 30%, respectively, under DNI conditions ($\alpha = 0^\circ$ and $\beta = 0^\circ$). The module transmittance increased as the α rotation angle increased, but when $|\alpha|$ exceeded 25°, the reflectance at the module incident surface increased, leading to a decrease in transmittance. The concentration efficiency at the CCPC end face was over 28% in the $|\alpha| < 15^\circ$ region, but when $|\alpha|$ exceeded 15°, the concentration efficiency decreased sharply. Through the simulation considering major experimental conditions such as illuminating device, fabrication, and assembly error of the optical module, and CCPC end to Si PV cell encapsulating condition, it was found that the light concentration efficiency to the Si PV incident surface decreased by approximately 8% in the $|\alpha| < 15^\circ$ region compared to the ideal optical module. The maximum light concentration efficiency to the Si PV incident surface is about 22% under the DNI conditions. Through experiments, the through-module transmittance and the generated power efficiency for α and β rotations were reviewed. While the through-module transmittance showed very similar rotation-dependent tendency and transmittance to the analysis results, the generated power efficiency showed approximately 54% of the calculated light concentration efficiency. These discrepancies were attributed to imperfect modeling of the applied illumination device, the shape of the proto-optical module, and assembly errors in attaching PV cells to the CCPC end surface. However, the rotation-dependent tendency of the generated power closely matched the analysis results. Therefore, we concluded that the functional characteristics of the proposed optical module were sufficiently validated.

The optical module proposed in this study is expected to have various positive effects contributing to the solar industry as a technology that enables both crop cultivation and solar power generation using solar energy. First, it is anticipated to positively impact food production by efficiently utilizing limited land resources to increase agricultural productivity. Moreover, an integrated system combining solar power generation and farming is expected to promote the establishment of sustainable agricultural management models and contribute to environmental protection. Additionally, the proposed technology is expected to promote diversification and innovation in the solar power generation industry, enhancing industrial competitiveness and contributing to the expansion of the renewable energy market. Overall, the results of this study suggest the possibility of opening up a more sustainable and efficient future through the integration of agriculture and energy industries.

Author Contributions: Conceptualization, B.-W.K. and W.-C.K.; methodology, B.-W.K. and B.-H.S.; investigation, J.J. and S.-W.L.; data curation, Y.-J.K., H.-S.S. and K.-J.K.; writing, J.J. and W.-C.K.; visualization, B.-H.S. and S.-W.L.; supervision, W.-C.K. All authors have read and agreed to the published version of the manuscript.

Funding: This work was supported by the National Research Foundation of Korea (NRF) grant funded by the Korean government (MSIT) (RS-2023-00250444).

Institutional Review Board Statement: Not applicable.

Informed Consent Statement: Not applicable.

Data Availability Statement: The raw data supporting the conclusions of this article will be made available by the authors on request.

Conflicts of Interest: Author Young-Jae Kim was employed by the company YNDK. Author Byung-Wook Kim was employed by the company Iproptics. The remaining authors declare that the research was conducted in the absence of any commercial or financial relationships that could be construed as a potential conflict of interest.

References

1. Maja, M.M.; Ayano, S.F. The Impact of Population Growth on Natural Resources and Farmers' Capacity to Adapt to Climate Change in Low-Income Countries. *Earth Syst. Environ.* **2021**, *5*, 271–283. [CrossRef]
2. *The World Population Prospects: The 2017 Revision*; The UN Department of Economic and Social Affairs: New York, NY, USA, 2017.
3. Raftery, A.E.; Alkema, L.; Gerland, P. Bayesian Population Projections for the United Nations. *Stat. Sci.* **2014**, *29*, 58–68. [CrossRef] [PubMed]
4. FAO. *How to Feed the World in 2050*; Food and Agriculture Organization: Rome, Italy, 2009. Available online: https://www.fao.org/fileadmin/templates/wsfs/docs/expert_paper/How_to_Feed_the_World_in_2050.pdf (accessed on 8 February 2024).
5. How Can Population and Resources Be Brought into Balance? Available online: https://www.millennium-project.org/challenge-3/ (accessed on 8 February 2024).
6. *FAO Statistical Yearbook 2021—World Food and Agriculture*; Food and Agriculture Organization of the United Nations: Rome, Italy, 2021. Available online: https://www.fao.org/documents/card/en?details=cb4477en (accessed on 8 February 2024).
7. De Oliveira, R.A.; Ramos, M.M.; De Aquino, L.A. Irrigation Management. In *Sugarcane: Agricultural Production, Bioenergy and Ethanol*; Academic Press: Cambridge, MA, USA, 2015; pp. 161–183.
8. Majeed, Y.; Khan, M.U.; Waseem, M.; Zahid, U.; Mahmood, F.; Majeed, F.; Sultan, M.; Raza, A. Renewable energy as an alternative source for energy management in agriculture. *Energy Rep.* **2023**, *10*, 344–359. [CrossRef]
9. Durga, N.; Schmitter, P.; Ringler, C.; Mishra, S.; Magombeyi, M.S.; Ofosu, A.; Pavelic, P.; Hagos, F.; Melaku, D.; Verma, S.; et al. Barriers to the uptake of solar-powered irrigation by smallholder farmers in sub-saharan Africa: A review. *Energy Strategy Rev.* **2024**, *51*, 101294. [CrossRef]
10. IEA. *Renewables 2023*; IEA: Paris, France, 2024. Available online: https://www.iea.org/reports/renewables-2023 (accessed on 9 February 2024).
11. Hossain, M.S.; Chowdhury, M.M.; Das, B.K. A sustainable energy approach for pumping and irrigation in the Barind Region of Bangladesh. In *Clean Techn Environ Policy*; Springer Science+Business Media: Berlin/Heidelberg, Germany, 2024. [CrossRef]
12. Toledo, C.; Scognamiglio, A. Agrivoltaic Systems Design and Assessment: A Critical Review, and a Descriptive Model towards a Sustainable Landscape Vision (Three-Dimensional Agrivoltaic Patterns). *Sustainability* **2021**, *13*, 6871. [CrossRef]
13. Widmer, J.; Christ, B.; Grenz, J.; Norgrove, L. Agrivoltaics, a promising new tool for electricity and food production: A systematic review. *Renew. Sustain. Energy Rev.* **2024**, *192*, 114277. [CrossRef]
14. Chalgynbayeva, A.; Balogh, P.; Szőllősi, L.; Gabnai, Z.; Apáti, F.; Sipos, M.; Bai, A. The Economic Potential of Agrivoltaic Systems in Apple Cultivation—A Hungarian Case Study. *Sustainability* **2024**, *16*, 2325. [CrossRef]
15. Jamil, U.; Bonnington, A.; Pearce, J.M. The Agrivoltaic Potential of Canada. *Sustainability* **2023**, *15*, 3228. [CrossRef]
16. Sarr, A.; Soro, Y.M.; Tossa, A.K.; Diop, L. Agrivoltaic, a Synergistic Co-Location of Agricultural and Energy Production in Perpetual Mutation: A Comprehensive Review. *Processes* **2023**, *11*, 948. [CrossRef]
17. Khandelwal, K.; Biswas, S.; Mishra, A.; Sharma, G.D. Semitransparent organic solar cells: From molecular design to structure–performance relationships. *J. Mater. Chem. C* **2022**, *10*, 13–43. [CrossRef]
18. Sheriff, H.K.M., Jr.; Li, Y.; Arneson, C.E.; Forrest, S.R. Reliability of colorfast semitransparent organic photovoltaics. *Device* **2024**, *2*, 100369. [CrossRef]
19. Zhao, N.; Zhen, T.; Wu, Y.; Wei, B.; Liao, Y.; Liu, Y. Efficient Semitransparent Organic Solar Cells Enabled by Ag Grid Electrodes and Optical Coupling Layers. *Nanomaterials* **2023**, *13*, 1308. [CrossRef] [PubMed]
20. Ghosh, B.K.; Jha, P.K.; Ghosh, S.K.; Biswas, T.K. Organic solar cells pros and cons: Outlooks toward semitransparent cell efficiency and stability. *AIP Adv.* **2023**, *13*, 020701. [CrossRef]

21. Amin, P.O.; Muhammadsharif, F.F.; Saeed, S.R.; Ketuly, K.A. A Review of the Improvements in the Performance and Stability of Ternary Semi-Transparent Organic Solar Cells: Material and Architectural Approaches. *Sustainability* **2023**, *15*, 12442. [CrossRef]
22. Bai, Y.; Han, F.; Tian, S.; Wang, F.; Jiang, S.; Wang, J.; Huang, T.; Tan, Z. Balance PCE, AVT and CRI for good eye comfort semi-transparent organic photovoltaics via Ga_2O_3 or In_2O_3 electron collection layers. *Org. Electron.* **2022**, *108*, 106572. [CrossRef]
23. Available online: https://www.synopsys.com/optical-solutions/lighttools/solar-design.html (accessed on 15 February 2024).
24. Hassan, H.U.; Nielsen, K.; Aasmul, S.; Bang, O. Polymer optical fiber compound parabolic concentrator tip for enhanced coupling efficiency for fluorescence based glucose sensors. *Biomed. Opt. Express* **2015**, *6*, 5008–5020. [CrossRef] [PubMed]
25. Chen, Y.T.; Lim, B.H.; Lim, C.S. General sun tracking formula for heliostats with arbitrarily oriented axes. *ASME J. Sol. Energy Eng.* **2006**, *128*, 245–250. [CrossRef]
26. Rajendran, P.; Smith, H. Modelling of solar irradiance and daylight duration for solar-powered UAV sizing. *Energy Explor. Exploit.* **2016**, *34*, 235–243. [CrossRef]

Disclaimer/Publisher's Note: The statements, opinions and data contained in all publications are solely those of the individual author(s) and contributor(s) and not of MDPI and/or the editor(s). MDPI and/or the editor(s) disclaim responsibility for any injury to people or property resulting from any ideas, methods, instructions or products referred to in the content.